applied sciences

MDPI

Article

Modeling for Spatial Overlap Effect of End-Pumped Passively Q-Switched Nd:YVO_4/Cr^{4+}:YAG Laser and Its Experimental Verification

Yueh-Chi Tu [1], Min-Xiang Hsieh [1], Hsing-Chih Liang [2] and Yan-Ting Yu [1,*]

[1] Department of Electrophysics, National Yang Ming Chiao Tung University, 1001 Ta-Hsueh Rd., Hsinchu 30010, Taiwan; doochy928@gmail.com (Y.-C.T.); iceattack000@gmail.com (M.-X.H.)
[2] Department of Optoelectronics and Materials Technology, National Taiwan Ocean University, Keelung 20224, Taiwan; hcliang@email.ntou.edu.tw
* Correspondence: kidddd1234.ep96g@gmail.com

Abstract: In this work, the spatial effects of the pumping and lasing were considered into the coupled rate equations of passively Q-switched lasers for the condition of no saturation in the gain medium. A transcendental equation of energy utilization was derived, and the solution to the equation was approximated by an analytic model developed in previous work. The reflection factor of output coupler with low reflectivity was modified for more accurate output energy evaluations. Experimentally, an end-pumped Nd:YVO_4/Cr^{4+}:YAG laser in a concave-plano cavity with output coupling reflectivity ranging from 10% to 92% was demonstrated, and two different pumping spot sizes of laser diode were adopted for validating the developed spatial model. The experimental results showed good agreements with the theoretical calculations.

Keywords: passively Q-switched; solid-state lasers; spatial overlap effect

Citation: Tu, Y.-C.; Hsieh, M.-X.; Liang, H.-C.; Yu, Y.-T. Modeling for Spatial Overlap Effect of End-Pumped Passively Q-Switched Nd:YVO_4/Cr^{4+}:YAG Laser and Its Experimental Verification. *Appl. Sci.* **2022**, *12*, 1338. https://doi.org/10.3390/app12031338

Academic Editor: Francesco Dell'Olio

Received: 29 October 2021
Accepted: 23 January 2022
Published: 27 January 2022

1. Introduction

Q-switched solid-state lasers manifest the capability of generating nanosecond-level pulses and high peak power light sources. Since the concept of Q-switching was proposed by Gordon Gould in 1958 and the first Q-switched device of ruby laser was demonstrated by R.W. Hellwarth and F.J. McClung in 1961 [1,2], there has been a wide range of applications to the fields of lidar, rangefinder, medicine, material processing, holography, and nonlinear optics [3–7]. The technique is achieved by tuning the intracavity losses of the resonator and can be further classified into active Q-switched (AQS) lasers and passive Q-switched (PQS) lasers. The operation of AQS lasers requires active control devices such as spinning mirrors, and acousto-optic attenuators to modulate the cavity losses. For PQS lasers, the saturable absorbers like Cr^{4+}:YAG for 1-μm lasers and V^{3+}:YAG for 1.3-μm lasers can be used to modulate the cavity losses; the crystals of these material are much lighter in comparison with the active control devices. Thus, PQS lasers possess the advantages of compactness, reliability, and light weight in the cavity design. Owing to the concern of reliability and cost reduction, PQS had been evaluated to be more applicable for the space mission in GLAS and MLA of NASA [8,9].

Since the coupled rate equations of passive Q-switching were proposed [10], several models and approaches of optimization have been developed. Many works have shown the dependence of performance on several factors in the cavity, such as the selection of gain medium, initial transmission of the absorber, reflectivity of output coupler, and intracavity mode area [11–15]. The transverse intensities of the pump and laser might affect the performance as well. In the classic PQS model, the transverse mode of lasing was assumed to be uniform. However, the mode of a resonator is more like a Hermite-Gaussian

distribution in real cases instead; thus, the influences of the spatial effect must be considered into the coupled rate equations.

In this article, we start from considering the lasing photon density to be a constant TEM_{00} Gaussian distribution along the optical direction and the pump density of a laser diode to be a top-hat distribution which diffracts along the optical direction, respectively, then incorporate the spatial dependence into the coupled rate equations for four-level PQS lasers. A transcendental equation of energy utilization is derived and approximated by an analytical function for calculating the output energy in the condition of no saturation in the gain crystal. To validate the developed spatially-dependent model, an end-pumped Nd:YVO_4/Cr^{4+}:YAG laser in a concave-plano cavity with output coupling reflectivity ranging from 10% to 92% was demonstrated, and two different pumping spot sizes of laser diode were adopted.

2. Modeling of Spatially Dependent PQS

The spatially-dependent lasing photon density and the population inversion density can be expressed as $\Phi(x,y,z) = \Phi\varphi_0(x,y,z)$ and $n(x,y,z) = Nr_0(x,y,z)$ where $\varphi_0(x,y,z)$ and $r_0(x,y,z)$ are the spatially-normalized lasing and pumping photon densities, respectively, Φ and N are the number of the photon in the cavity and the number of the inversion population in the gain medium. For a single fundamental transverse TEM_{00} mode, the lasing photon density can be expressed as:

$$\varphi_0(x,y,z) = \frac{2}{\pi w_c^2 l_c} e^{-2(x^2+y^2)/w_c^2} \tag{1}$$

$$w_c = w_0\sqrt{1+\left(\frac{\lambda z}{\pi w_0^2}\right)^2} \approx w_0\sqrt{1+\left(\frac{\lambda d_c}{\pi w_0^2}\right)^2} \tag{2}$$

where l_c is the length of the cavity, w_c is the mode size in the gain crystal, w_0 is the beam waist of lasing, d_c is the distance from the beam waist to the middle of the length of the gain crystal, and λ is the wavelength of lasing. We assume a constant beam size without diffraction here if the variation of the beam size in the gain medium is small enough and neglectable. For a fiber-coupled laser diode pumping, the population inversion density in the gain medium can be described as a top-hat distribution [16,17]:

$$r_0(x,y,z) = \frac{\delta e^{-\delta z}}{\pi w_p^2\left(1-e^{-\delta l_g}\right)} \cdot \mathrm{H}\left[w_p^2 - \left(x^2+y^2\right)\right] \cdot \mathrm{H}(l_g - z) \tag{3}$$

$$w_p = w_{p0}\sqrt{1+\left[\frac{\lambda_p M_p^2}{n_r \pi w_{p0}^2}(z-z_0)\right]^2} \tag{4}$$

where δ is the absorption coefficient at the wavelength of the pumping source, l_g is the length of the gain crystal, w_p is the pump size in the gain crystal, H is the Heaviside step function, w_{p0} is the beam waist of the pump, λ_p is the wavelength of the pump, M_p^2 is the beam quality factor, n_r is the refractive index of the gain crystal, and z_0 is the location of the focal plane of the pump. We introduce the spatial dependence stated above to the coupled rate equations of the four-level PQS laser. The coupled rate equations can be expressed as:

$$\frac{d\Phi}{dt}\varphi_0 = \frac{\Phi}{t_r}\varphi_0\left[2\sigma N r_0 l_g - \frac{2\sigma_{gs}N_{gs}l_s}{V_s} - \frac{2\sigma_{es}N_{es}l_s}{V_s} - \ln\left(\frac{1}{R_{oc}}\right) - L_s\right] \tag{5}$$

$$\frac{dN}{dt}r_0 = -\gamma\frac{2l_c\sigma}{t_r}\Phi N\varphi_0 r_0 \tag{6}$$

$$\frac{dN_{gs}}{dt} = -\frac{A}{A_s}\frac{2l_c\sigma_{gs}N_{gs}}{t_r}\Phi\varphi_0 \tag{7}$$

where σ is the stimulated emission cross section of the gain medium, σ_{gs} and σ_{es} are the ground-state and excited-state absorption cross section of the absorber, N_{gs} and N_{es} are the number of the population in the ground state and in the excited state of the absorber, l_g and l_s are the lengths of the gain medium and the absorber respectively, V_s is the volume of the absorber, R_{oc} is the output coupler reflectivity, L_s is the dissipative loss in a roundtrip for a photon, t_r is the roundtrip time for a photon in the cavity, γ is the inversion reduction factor, and A and A_s are the cross areas of lasing in the gain medium and in the absorber, respectively. According to the Lambert-Beer absorption law, the initial transmission of the absorber can be expressed as $T_0 = \exp\left(-\sigma_{gs} N_{so} l_s / V_s\right)$ where $N_{so} = N_{gs} + N_{es}$. By integrating coupled rate equations with respect to the cavity volume, we have

$$\frac{d\Phi}{dt} = \frac{\Phi}{t_r}\left[\frac{2\sigma N l_g}{V_{eff}} - \frac{2\sigma_{gs} N_{gs} l_s}{V_s} - \frac{2\sigma_{es} N_{es} l_s}{V_s} - \ln\left(\frac{1}{R_{oc}}\right) - L_s\right] \tag{8}$$

$$\frac{dN}{dt} = -\gamma \frac{2 l_c \sigma N \Phi}{t_r V_{eff} S} \tag{9}$$

$$\frac{dN_{gs}}{dt} = -\frac{A}{A_s}\frac{2 l_c \sigma_{gs} N_{gs} \Phi}{t_r V_{eff} S} \tag{10}$$

where the effective mode volume V_{eff} and the overlap efficiency S

$$V_{eff} = \left[\int r_0(x,y,z)\varphi_0(x,y,z)dV\right]^{-1} = \left[\frac{G(1)}{\pi l_g\left(1 - e^{-\delta l_g}\right)}\right]^{-1} \tag{11}$$

$$S = \frac{\left[\int r_0(x,y,z)\varphi_0(x,y,z)dV\right]^2}{\left[\int r_0(x,y,z)\varphi_0^2(x,y,z)dV\right]} = \frac{w_c^2 [G(1)]^2}{\left(1 - e^{-\delta l_g}\right) G(2)} \tag{12}$$

$$G(m) = \delta \int_{d_c - \frac{l_g}{2}}^{d_c + \frac{l_g}{2}} \left(1 - e^{-2m w_p^2 / w_c^2}\right) \frac{e^{-\delta[l_g - (z - z_0)]}}{w_p^2} dz \tag{13}$$

From Equation (8), with the condition that $d\Phi/dt = 0$ and $N_{es} = 0$, the initial population in the gain medium for generating a pulse is given by

$$N_i = \frac{V_{eff}}{2\sigma l_g}\left[\ln\left(\frac{1}{T_0^2}\right) + \ln\left(\frac{1}{R_{oc}}\right) + L_s\right] \tag{14}$$

Dividing the Equation (9) by the Equation (10) and integrating the result can give N_{gs} as a function of N, that is $N_{gs} = N_{so}(N/N_i)^{\alpha}$ where $\alpha = A\sigma_{gs}/(\gamma A_s \sigma)$. Dividing the rate Equation (8) by the rate Equation (9) and using the Equation (14) give

$$\frac{d\Phi}{dN} = \frac{S l_g}{\gamma l_c}\left[-1 + \frac{(N_i - N_t)}{N_i}\left(\frac{N}{N_i}\right)^{\alpha - 1} + \frac{N_t}{N}\right] \tag{15}$$

where

$$N_t = \frac{V_{eff}}{2\sigma l_g}\left[\beta \ln\left(\frac{1}{T_0^2}\right) + \ln\left(\frac{1}{R_{oc}}\right) + L\right] \tag{16}$$

and $\beta = \sigma_{es}/\sigma_{gs}$. The second derivative of Φ with respect to N can be expressed as

$$\frac{d^2\Phi}{dN^2} = -\frac{S l_g}{\gamma l_c}\left[1 - (\alpha - 1)\frac{(N_i - N_t)}{N_i}\left(\frac{N}{N_i}\right)^{\alpha - 2} + \frac{N_t}{N^2}\right] \tag{17}$$

The condition $d^2\Phi/dN^2 > 0$ at $N = N_i$ is referred to as the second threshold for generating a stable pulse train in PQS lasers and can be given by $\xi > \alpha/(\alpha - 1)$ where $\xi = N_i/N_t$ is the ratio of the initial inversion to the critical inversion. Integrating the equation of $d\Phi/dN$ yields

$$\Phi(N) = \frac{Sl_g}{\gamma l_c}\left[(N_i - N) - \frac{(N_i - N_t)}{\alpha}\left[1 - \left(\frac{N}{N_i}\right)^{\alpha}\right] - N_t \ln\left(\frac{N_i}{N}\right)\right] \tag{18}$$

The final inversion population N_f can be determined by the condition $\Phi\left(N_f\right) = 0$:

$$\left(N_i - N_f\right) - \frac{N_i - N_t}{\alpha}\left[1 - \left(\frac{N_f}{N_i}\right)^{\alpha}\right] - N_t \ln\left(\frac{N_i}{N_f}\right) = 0 \tag{19}$$

Defining $\eta_E = \left(N_i - N_f\right)/N_i$ as the energy-utilization factor, the Equation (19) can be expressed as a transcendental equation:

$$\eta_E - \alpha^{-1}\left(1 - \xi^{-1}\right)\left[1 + (1 - \eta_E)^{\alpha}\right] - \xi^{-1}\ln(1 - \eta_E) = 0 \tag{20}$$

In the condition of no gain saturation, the larger value of the η_E means the more efficient population depleted in the saturable absorber, since η_E cannot be directly solved as a function of ξ and α. A powerful expression derived from numerical fitting [18] for the energy utilization efficiency η_E is given by

$$\eta_E(\xi, \alpha) = 1 - \exp\left[-1.55\left(\frac{\alpha^2 - 1}{\alpha}\right)\left(\xi - \frac{\alpha}{\alpha - 1}\right)^{0.85}\right] \tag{21}$$

with $\xi > \alpha/(\alpha - 1)$. The transcendental equation quantitatively determines the characteristics of PQS. The output energy can be expressed as

$$E_{out} = \frac{h\nu_l}{t_r}(1 - R_{oc})\int_{t_i}^{t_f}\Phi dt = \frac{h\nu_l A_{eff} S}{2\sigma\gamma}(1 - R_{oc})\ln\left(\frac{1}{1 - \eta_E(\xi, \alpha)}\right) \tag{22}$$

where $h\nu_l$ is the lasing photon energy and A_{eff} is the effective mode area that is equal to V_{eff}/l_c. The transmittance of output coupler can be well approximated to be $\ln(1/R_{oc})$ for high reflectivity. However, for those reflectivity lower than e^{-1}, it is more general and appropriate to use $(1 - R_{oc})$ term for a wide range of reflectivity [18]. So far, we have completed the derivation of the output energy equation, and the term A_{eff} and S in the Equation (22) show the significance of considering the spatial effect. Without considering the effect, the energy factor term would be $h\nu_l A/(2\sigma\gamma)$ according to the previous works, where A is the mode size area in the gain medium.

3. Experimental Setup and Theoretical Fitting

To verify the model, we set up a concave-plano cavity for the PQS operation, and the experimental scheme is shown in Figure 1. The pumping source was a fiber-coupled laser diode with a core diameter of 0.2 mm, which was able to offer a maximum power of 40 W at 808 nm. The pumping energy from the laser diode was configured as pulse-pumping with the frequency 10 kHz and duty cycle 30% for reducing the thermal lensing effect. The input side of the resonator was a concave mirror with a radius of curvature 30 mm, and its entrance facet was coated anti-reflection films at 808 nm with reflectivity less than 0.1%; the second facet was coated high-reflection films at 1064 nm with reflectivity 99.8% and transmittance 96% at 808 nm. Since our model was based on the condition of no gain saturation, we chose a low-doped concentration 0.3 at. % Nd:YVO_4 as the gain medium to avoid saturation cases. Furthermore, the gain medium was an a-cut rectangular crystal

with the dimensions of $3 \times 3 \times 6$ mm^3, and both ends were coated anti-reflection films at 1064 nm with reflectivity less than 0.1%. The saturable absorbers were two Cr^{4+}:YAG with the initial transmission $T_0 = 35\%$ and 50%, and both were rectangular crystals with the dimensions of $3 \times 3 \times 3$ mm^3. The coating for the absorbers on both ends were the same as those of the gain medium. The gain medium and the saturable absorbers were wrapped with indium foils and mounted in copper holders that were connected to a water-cooling system keeping a temperature of 22 °C. The indium foils were used as high-efficiency heat sinks and filling material for tiny gaps between the crystal and the holder. Several flat mirrors with different reflectivity R_{oc} in a range from 10% to 92% were employed as the output couplers in this experiment. The distance d_c in Figure 1 is the average distance from the output coupler to the gain crystal, and d_s is the distance from the output coupler to the absorber.

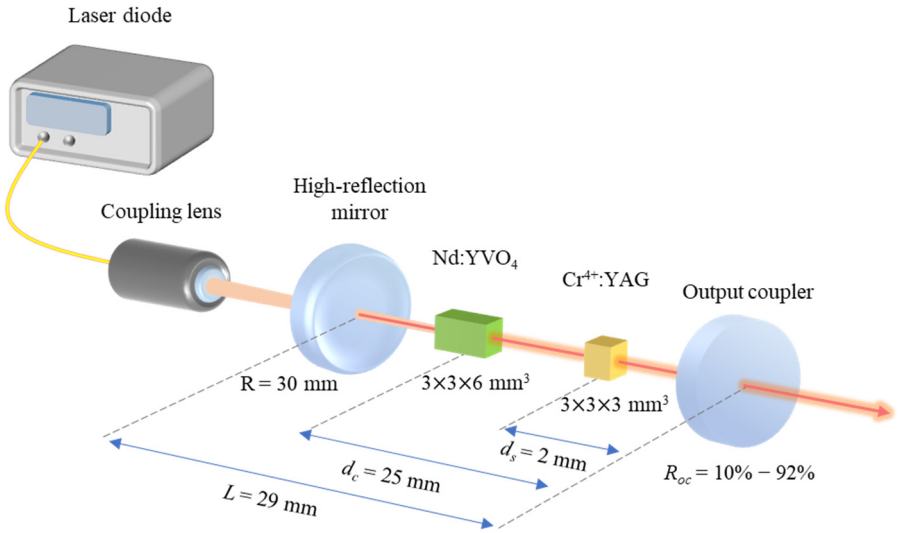

Figure 1. Schematic of an concave-plano resonator of a PQS solid-state laser.

The cavity length was set to be 29 mm to satisfy the criterion of the second threshold condition. By $w(d) = w_0\sqrt{1 + (\lambda d/\pi w_0^2)^2}$, the mode sizes of the two ends and the middle point in the gain crystal can be evaluated to be 0.180 mm^2, 0.226 mm^2, and 0.202 mm^2 by substituting the $d = 28$ mm, 22 mm, and 25mm, respectively. In modeling, we assumed the variation of the mode size in the crystal is small, then we ignored the effect of diffraction inside the gain crystal. Since the mode size in the middle is very close to the average mode size of the two ends, the approximation still holds in this case, so here we take $w_c = 0.226$ mm^2. By the experimental conditions that $d_s = 2$ mm, the mode sizes w_s in the saturable absorber can be obtained to be 0.046 mm. Adding the spontaneous emission coefficient of the gain crystal $\sigma = 15.6 \times 10^{-19}$ cm^2 and the absorption coefficient of the ground state of the absorber $\sigma_{gs} = 8.7 \times 10^{-19}$ cm^2, the value of α can be evaluated to be $\alpha = 11$.

To investigate the influence of the spatial overlap effect on the output energy, two sets of focusing lens were adopted for different scales of beam expansion. Consequently, the average pump beam radii of 0.1 mm and 0.3 mm were reimaged into the gain crystal with 90% coupling efficiency, respectively. Given the following experimental parameters $d_c = 25$ mm, $l_g = 6$ mm, $z_0 = 25$ mm, $\lambda_p = 808$ nm, $\delta = 0.12$ mm^{-1}, $n_r = 2.22$, $w_c = 0.202$ mm, the integration in Equation (13) can be evaluated numerically, then substitute the result into the Equations (11) and (12) to obtain the effective mode area and overlap efficiency $A_{eff} = 0.344$ mm^2 and $S = 0.292$ for the pump size $w_p = 0.1$ mm, $A_{eff} = 2.883$ mm^2, and $S = 0.264$ for $w_p = 0.3$ mm. Adding the inversion reduction factor

$\gamma = 1$, the output energy factor $h\nu_l A_{eff} S/(2\sigma\gamma)$ can be evaluated to be 52 μJ and 65 μJ. We will discuss the experimental results in the following section.

4. Results and Discussions

Figure 2 shows the plot of the average output power versus the input power in the pulse pumping scheme for $T_0 = 35\%$ and 50% with the output coupler $R_{oc} = 40\%$. The results show a characteristic staircase structure where the plateaus indicate the locking effect at various simple frequency ratio. This phenomenon is consistent with the previous results [19].

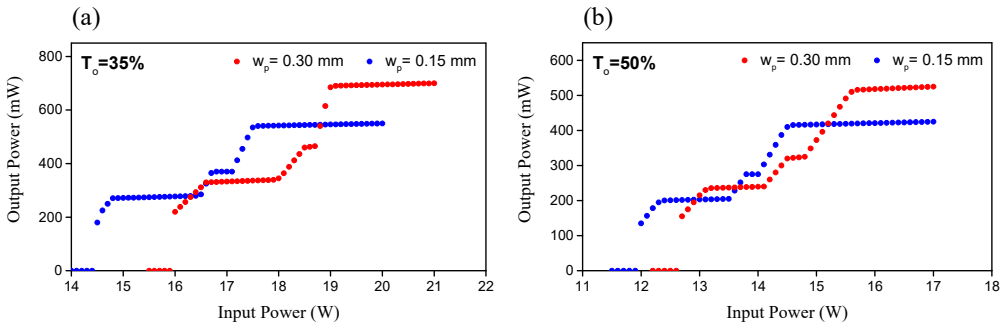

Figure 2. The plot of the output power versus the input power of two pumping foci with the initial transmission (**a**) 35% and (**b**) 50% of the saturable absorbers.

Figure 3 shows a typical stable pulse train and the pulse width of a single pulse with time span division of 8 ms and 40 ns in the case of $T_0 = 35\%$ to the frequency-locked states of 1:1, i.e., f_{rep} = 10 KHz. The overall pulse-to-pulse amplitude fluctuation was found to be within 5%. The pulse duration was measured approximately to be 2 ns, as shown in Figure 3b. We also observed that there was no additional pulse or satellite pulse in every single Q-switched shot.

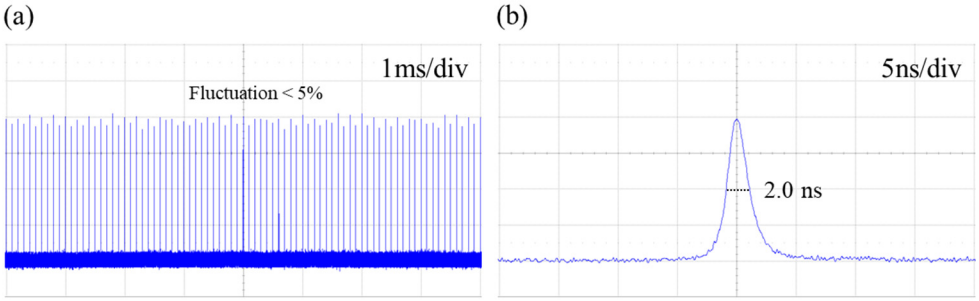

Figure 3. (**a**) A stable pulse train with fluctuation deviation less than 5%. (**b**) A single pulse of 2 nanoseconds generated by a PQS Nd:YVO_4/Cr^{4+}:YAG laser.

The output energy versus the output coupler reflectivity of the theoretical fitting and the experimental results with $T_0 = 35\%$ for two pumping foci are shown in Figure 4a. It can be clearly seen that the values of the curve of the case $w_p = 0.3$ mm is higher than that of the case $w_p = 0.1$ mm by a factor of 1.25 on average, which is exactly corresponding to the ratio of the energy factor 65 μJ to the energy factor 52 μJ. The results for other cases of $T_0 = 50\%$ is also shown in Figure 4b. The agreement of the theoretical calculations and the experimental data confirms the validity of the developed spatial model.

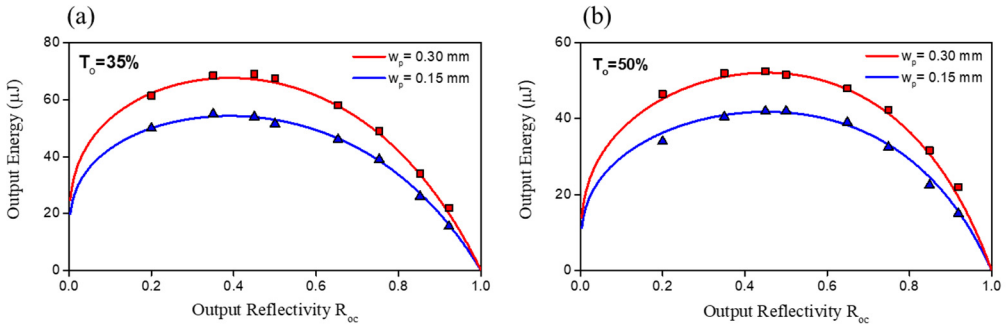

Figure 4. Theoretical fitting and experimental results of the output energy of the two pumping foci $w_p = 0.1$ mm and $w_p = 0.3$ mm with (**a**) $T_0 = 35\%$ and (**b**) $T_0 = 50\%$.

By the condition $d\Phi/dN = 0$ from Equation (12), the inversion population when the maximum photon number occurs is almost equal to N_t in our cases with $\alpha = 11$. Thus, the spatially dependent peak power of the PQS model can be evaluated by

$$P_{peak} = \frac{h\nu_l}{t_r}(1 - R_{oc})\Phi(N_t) \tag{23}$$

and the space-related terms S and V_{eff} are included in the maximum photon number $\Phi(N_t)$. The theoretical fitting and experimental results for the peak powers are shown in the Figure 5 for the cases $w_p = 0.1$ mm and $w_p = 0.3$ mm with $T_0 = 35\%$. The peak powers for both pumping foci possess the similar pattern to that of the output energies owing to the spatial overlap effect too. From that, again, we see the good agreement between the theoretical fitting and experimental results.

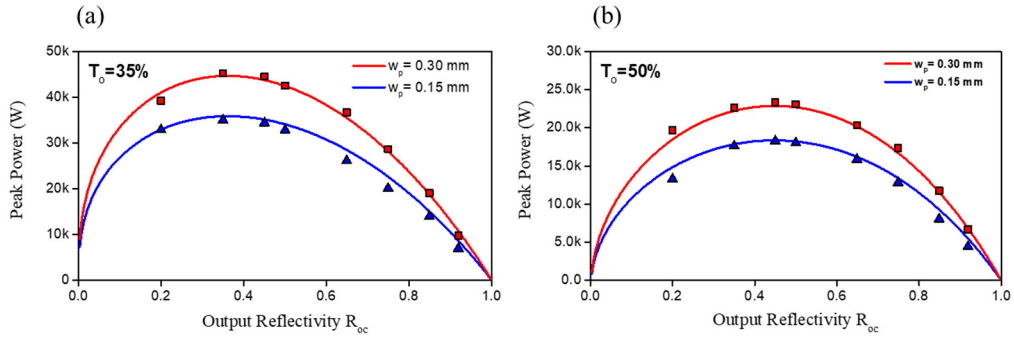

Figure 5. Theoretical fitting and experimental results of the peak power of the two pumping foci $w_p = 0.1$ mm and $w_p = 0.3$ mm with (**a**) $T_0 = 35\%$ and (**b**) $T_0 = 50\%$.

The above result and discussion are based on the ratios of the output frequency to the input frequency to be 1:1, which means that the input energy during one pulse-pumping cycle is enough to generate a corresponding lasing pulse. From the experimental results, we find that the model is still valid at various simple frequency ratios such as 1:2 and 2:3, which is the frequency locking effect as the first and second plateau shown in Figure 2. The time-domain pulse train is shown in Figure 6 for the case that $w_p = 0.1$ mm, $T_0 = 35\%$, $R_{oc} = 40\%$ with pulse-pumping frequency 10 kHz, and the output energy factor $h\nu_l A_{eff} S/(2\sigma\gamma)$ for the pump size is still around 52 μJ.

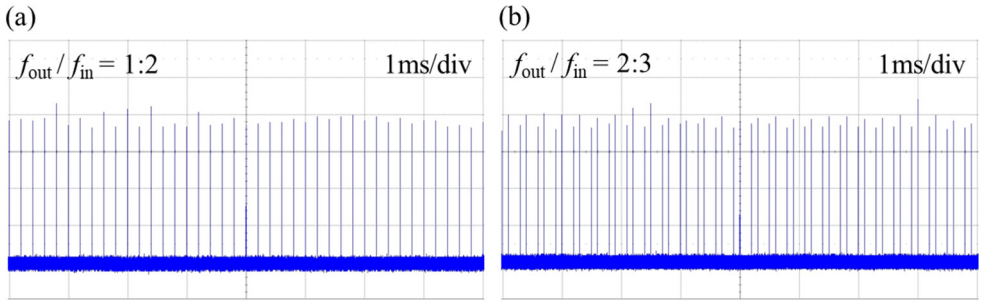

Figure 6. The pulse trains at frequency ratios (**a**) f_{out}/f_{in} = 1/2 and (**b**) f_{out}/f_{in} = 2/3 for the case $w_p = 0.1$ mm, $T_0 = 35\%$, $R_{oc} = 40\%$ with pulse-pumping frequency 10 kHz.

5. Conclusions

We have considered the spatial dependency of the laser and the pump into the coupled rate equations for an end-pumped four-level PQS laser in the condition of no gain saturation, then derived an expression for calculating the output energy. The experimental setup for verifying the model has been demonstrated. The good agreements of the theoretical fittings and experimental results on the output energy and the peak power have validated the accuracy of the model.

Author Contributions: Conceptualization, Y.-C.T. and M.-X.H.; validation, Y.-C.T. and M.-X.H.; formal analysis, M.-X.H. and H.-C.L.; resources, Y.-C.T.; writing—original draft preparation, Y.-C.T.; writing—review and editing, H.-C.L. and Y.-T.Y.; supervision, H.-C.L. and Y.-T.Y. All authors have read and agreed to the published version of the manuscript.

Funding: This work was supported by the Ministry of Science and Technology of Taiwan (Contract No. 109-2119-M-009-015-MY3).

Data Availability Statement: All of the data reported in the paper are presented in the main text. Any other data will be provided on request.

Conflicts of Interest: The authors declare no conflict of interest.

References

1. Taylor, N. *LASER: The Inventor, the Nobel Laureate, and the Thirty-Year Patent War*; Simon & Schuster: New York, NY, USA, 2002.
2. McClung, F.J.; Hellwarth, R.W. Giant optical pulsations from ruby. *Appl. Opt.* **1962**, *1*, 103–105. [CrossRef]
3. Zayhowski, J.J. Passively Q-switched Nd:YAG microchip lasers and applications. *J. Alloys Compd.* **2000**, *303*, 393–400. [CrossRef]
4. De Young, R.J.; Barnes, N.P. Profiling atmospheric water vapor using a fiber laser lidar system. *Appl. Opt.* **2010**, *49*, 562–567. [CrossRef] [PubMed]
5. Skorczakowski, M.; Swiderski, J.; Pichola, W.; Nyga, P.; Zajac, A.; Maciejewska, M.; Galecki, L.; Kasprzak, J.; Gross, S.; Heinrich, A.; et al. Mid-infrared Q-switched Er:YAG laser for medical applications. *Laser Phys. Lett.* **2010**, *7*, 498. [CrossRef]
6. Meier, M.; Romano, V.; Feurer, T. Material processing with pulsed radially and azimuthally polarized laser radiation. *Appl. Phys. A* **2007**, *86*, 329–334. [CrossRef]
7. Harigel, G.; Baltay, C.; Bregman, M.; Hibbs, M.; Schaffer, A.; Bjelkhagen, H.; Hawkins, J.; Williams, W.; Nailor, P.; Michaels, R.; et al. Pulse stretching in a Q-switched ruby laser for bubble chamber holography. *Appl. Opt.* **1986**, *25*, 4102–4110. [CrossRef] [PubMed]
8. Krebs, D.J.; Novo-Gradac, A.M.; Li, S.X.; Lindauer, S.J.; Afzal, R.S.; Anthony, W.Y. Compact, passively Q-switched Nd: YAG laser for the MESSENGER mission to Mercury. *Appl. Opt.* **2005**, *44*, 1715–1718. [CrossRef] [PubMed]
9. Afzal, R.S.; Anthony, W.Y.; Dallas, J.L.; Melak, A.; Lukemire, A.T.; Ramos-Izqueirdo, L.; Mamakos, W. The geoscience laser altimeter system (GLAS) laser transmitter. *IEEE J. Sel. Topics Quantum Electron.* **2007**, *13*, 511–536. [CrossRef]
10. Szabo, A.; Stein, R.A. Theory of laser giant pulsing by a saturable absorber. *J. Appl. Phys.* **1965**, *36*, 1562–1566. [CrossRef]
11. Degnan, J.J. Optimization of passively Q-switched lasers. *IEEE J. Quantum Electron.* **1995**, *31*, 1890–1901. [CrossRef]
12. Xiao, G.; Bass, M. A generalized model for passively Q-switched lasers including excited state absorption in the saturable absorber. *IEEE J. Quantum Electron.* **1997**, *33*, 41–44. [CrossRef]
13. Chen, Y.P.; Lan, Y.P.; Chang, H.L. Analytical model for design criteria of passively Q-switched lasers. *IEEE J. Quantum Electron.* **2001**, *37*, 462–468. [CrossRef]
14. Pavel, N.; Saikawa, J.; Kurimura, S.; Taira, T. High average power diode end-pumped composite Nd: YAG laser passively Q-switched by Cr4+: YAG saturable absorber. *Jpn. J. Appl. Phys.* **2001**, *40*, 1253. [CrossRef]

15. Tuan, P.H.; Chang, C.C.; Chang, F.L.; Lee, C.Y.; Sung, C.L.; Cho, C.Y.; Chen, Y.F.; Su, K.W. Modelling end-pumped passively Q-switched Nd-doped crystal lasers: Manifestation by a Nd: YVO 4/Cr 4+: YAG system with a concave-convex resonator. *Opt. Express* **2017**, *25*, 1710–1722. [CrossRef] [PubMed]
16. Chen, Y.F. cw dual-wavelength operation of a diode-end-pumped Nd: YVO4 laser. *Appl. Phys. B.* **2000**, *70*, 475–478. [CrossRef]
17. Huang, Y.J.; Tzeng, Y.S.; Tang, C.Y.; Chen, Y.F. Efficient dual-wavelength synchronously mode-locked picosecond laser operating on the 4 F 3/2→ 4 I 11/2 transition with compactly combined dual gain media. *IEEE J. Sel. Top. Quantum Electron.* **2014**, *21*, 56–62. [CrossRef]
18. Chen, Y.F.; Hsieh, M.X.; Tu, Y.C.; Lee, C.C.; Yu, Y.T.; Tsou, C.H.; Liang, H.C. Pedagogically fast model to evaluate and optimize passively Q-switched Nd-doped solid-state lasers. *Opt. Lett.* **2021**, *46*, 1588–1591. [CrossRef] [PubMed]
19. Chen, Y.F.; Chien, P.Y.; Lee, C.C.; Huang, K.F.; Liang, H.C. Timing jitter reduction of passively Q-switched solid-state lasers by coupling resonance between pumping and firing rates. *Opt. Lett.* **2020**, *45*, 2902–2905. [CrossRef] [PubMed]